Journal of Solid State Chemistry 183 (2010) 1186–1193

Contents lists available at ScienceDirect

Journal of Solid State Chemistry

journal homepage: www.elsevier.com/locate/jssc

Synthesis and crystal structure of $Ln_2M^{2+}Ge_4O_{12}$, Ln=rare-earth element or Y; M=Ca, Mn, Zn

Vladimir G. Zubkov, Nadezda V. Tarakina *, Ivan I. Leonidov, Alexander P. Tyutyunnik, Ludmila L. Surat, Marina A. Melkozerova, Elena V. Zabolotskaya, Dina G. Kellerman

Institute of Solid State Chemistry, Ural Branch of the Russian Academy of Sciences, 91 Pervomayskaya str., Ekaterinburg, 620990, Russia

ARTICLE INFO

Article history:
Received 27 October 2009
Received in revised form
8 March 2010
Accepted 16 March 2010
Available online 20 March 2010

Keywords:
Rare-earth luminescent materials
Crystal structure
Germanates
X-ray powder diffraction

ABSTRACT

The crystal structure of the promising optical materials $Ln_2M^{2+}Ge_4O_{12}$, where Ln=rare-earth element or Y; M=Ca, Mn, Zn and their solid solutions has been studied in detail. The tendency of rare-earth elements to occupy six- or eight-coordinated sites upon iso- and heterovalent substitution has been studied for the $Y_{2-x}Er_xCaGe_4O_{12}$ (x=0–2), $Y_{2-2x}Ce_xCa_{1+x}Ge_4O_{12}$ (x=0–1), $Y_2Ca_{1-x}Mn_xGe_4O_{12}$ (x=0–1) and $Y_{2-x}Pr_xMnGe_4O_{12}$ (x=0–0.5) solid solutions. A complex heterovalent state of Eu and Mn in $Eu_2MnGe_4O_{12}$ has been found.

1. Introduction

One of the main goals of modern research in materials science is the synthesis and development of new materials promising for application in photonics. Recent achievements in this field were summarized in Refs. [1,2]. However some aspects and some groups of promising materials remained untouched by the authors. Among them are the germanates $Ln_2M^{2+}Ge_4O_{12}$, Ln=rare-earth element or Y with cyclic anion groups $[Ge_4O_{12}]^{8-}$.

The optical properties of these germanates strongly depend on their chemical composition and crystal structure features. For the case M=Cu, the $Ln_2Cu^{2+}Ge_4O_{12}$, Ln=Eu–Lu, Y^{3+}, compounds crystallize in a triclinic unit cell (S.G. $P-1$, Z=1) [3–5]. Their crystal structure consists of layers with discrete $[Ge_4O_{12}]^{8-}$ anions, in which four GeO_2 groups (oxygen atoms are located above and under the plane of the cycle) are connected to each other by means of Ge–O–Ge bridge bonds. Between the layers Cu^{2+} (coordination number=4) and Ln^{3+} (coordination number=7) ions are located. The crystal structure implies the presence of specific features in the IR and Raman spectra, e.g. in-phase vibrations inside the cycle which result in the appearance of collective vibration modes [6]. In addition, high fluorescence has been observed under Nd:YAG laser excitation (λ=1064 nm). However, the origin of the fluorescence has not been revealed yet. It is worth to mention that the silicates $Ln_2Cu^{2+}Si_4O_{12}$, where Ln=Eu–Lu or Y^{3+}, have been synthesized as well, but their crystal structure and properties have not been studied yet [7].

For the case M=Ca, the $Ln_2Ca^{2+}Ge_4O_{12}$ compounds, where Ln=Y, Gd, Ho, Er, Yb [8,9], crystallize in S.G. *P4/nbm*, Z=2, exhibiting similar cycles in the structural motive. Layers of discrete $[Ge_4O_{12}]^{8-}$ cycles alternate with layers of metal atoms (1/2Ca+1/2Ln) in distorted octahedral coordination and Ln in square antiprism coordination. As it has been shown in our previous works [10,11], these compounds have an optical gap ΔE of about ~4.95(5) eV. Intense fluorescence in $Ln_2CaGe_4O_{12}$, Ln=Er^{3+} and Ho^{3+}, caused by $^4I_{13/2} \Rightarrow {}^4I_{15/2}$ and $^5I_6 \Rightarrow {}^5I_8$ transitions, respectively, has been found under IR laser (λ=976 nm) excitation [11]. The compound $CeMn_2Ge_4O_{12}$, in which Mn^{2+} and Ce^{4+} are placed in distorted octahedral and square antiprism coordination, respectively, has an analogous structure [12].

Thus, taking all of the above into account, the $Ln_2M^{2+}Ge_4O_{12}$ (Ln=rare-earth element or Y, M=Ca, Cu, Mn) compounds are promising for use as optical hosts, in which different rare-earth elements can be introduced as a sensitizer or activator. The main goal of the present work is to complete previous crystal structure investigations by a detailed crystal structure study of manganese cyclogermanates and different solid solutions, checking the possibility of iso- and heterovalent substitutions in the $Ln_2M^{2+}Ge_4O_{12}$ (Ln=rare-earth element or Y, M=Ca, Mn, Zn) matrix, in order to optimize their chemical composition in relation to optical properties.

2. Experiment

$Ln_2M^{2+}Ge_4O_{12}$ and solid solutions, where Ln=rare-earth element or Y; M=Ca, Mn, Zn, were synthesized in air from

* Corresponding author. Fax: +7 343 3744495.
E-mail address: tarakina@ihim.uran.ru (N.V. Tarakina).

0022-4596/$ - see front matter © 2010 Elsevier Inc. All rights reserved.
doi:10.1016/j.jssc.2010.03.027

stoichiometric mixtures of Ln_2O_3 (Ln=Eu, Gd, Dy, Ho, Er, Tm, Yb, Lu, Y) (99.99%), $CaCO_3$ (99.9%), Mn_2O_3 (99.9%), ZnO (99.9%) and GeO_2 (99.9%) by annealing with heating in conventional and microwave furnaces. To obtain calcium germanates $Ln_2CaGe_4O_{12}$ (Ln=Eu, Gd, Dy, Ho, Er, Tm, Yb, Lu, Y) in a conventional heating furnace stoichiometric mixtures of oxides were first annealed at 950 °C for 10 hours, then pressed into pellets and heated in the furnace up to 1100 °C and annealed at this temperature for 150 hours with intermediate cooling and regrinding in an agate mortar every 20 hours. In a microwave furnace calcium cyclogermanates have been obtained after 12 hours of annealing at 1050 °C with intermediate cooling and regrinding every 4 hours. $Ln_2MnGe_4O_{12}$ (Ln=Eu, Gd, Dy, Ho, Er, Tm, Yb, Lu, Y) have been obtained from stoichiometric mixtures of oxides placed in a conventional furnace at 1050 °C, annealed for 100 hours with intermediate quenching in air and regrinding in an agate mortar every 20 hours. As for calcium cyclogermanates the application of a microwave field allowed a reduction of the annealing time by a factor of twelve, the single phase $Ln_2MnGe_4O_{12}$ (Ln=Eu, Gd, Dy, Ho, Er, Tm, Yb, Lu, Y) was obtained at a temperature of 1050 °C during 8 hours.

X-ray powder diffraction (XRD) patterns were collected at room temperature on a transmission STADI-P (STOE, Germany) diffractometer equipped with a linear mini-PSD detector, using Cu$K\alpha_1$ radiation in the 2θ range 2°–120° with a step of 0.02°. Polycrystalline silicon (a=5.43075(5) Å) was used as external standard. The phase purity of the samples was checked by comparing their XRD patterns with those in the Powder diffraction file-PDF2 database (ICDD, USA, release 2009). The crystal structure has been refined with the GSAS program suite [13] using the X-ray powder diffraction data.

For the transmission electron microscopy (TEM) studies the samples were crushed in ethanol. A drop of this suspension was put on a copper grid covered with a holey carbon film. Electron diffraction (ED) patterns were obtained using a Philips CM20 operated at 200 kV. The energy dispersive X-ray (EDX) microanalysis was performed in a JEOL JSM6390 LA scanning electron microscope equipped with the EDX JED-2300 system.

Magnetic susceptibility was measured by a MPMS-5XL (Quantum Design) SQUID-magnetometer at the field H=100 and 1000 Oe in the temperature range of 1.5–300 K.

Electron spin resonance (ESR) spectra were collected at room temperature on an X-band CMS 8400 spectrometer (ADANI, Belarus) in magnetic fields 0–0.55 T.

3. Results and discussion

3.1. Crystal structure of $Ln_2M^{2+}Ge_4O_{12}$, where Ln=rare-earth element or Y; M=Ca, Mn

Selected area electron diffraction patterns, viewed along the [1 0 0] and [0 0 1] zone axes and the XRD pattern of $Ho_2CaGe_4O_{12}$ are shown in Fig. 1, they are representative for the diffraction patterns of all other synthesized germanates (Supporting Materials 1). An analysis of systematically absent reflections (hk0: $h+k=2n$; 0kl: $k=2n$; h00: $h=2n$) in XRD and ED patterns indicates the $P4/nbm$ space group for all compounds. For several samples a trace quantity of the impurity phase $Ln_2Ge_2O_7$ has been observed.

The unit cell parameters of the $Ln_2M^{2+}Ge_4O_{12}$ compounds, where Ln=rare-earth element or Y; M=Ca, Mn, smoothly decrease with decreasing radius of the rare-earth elements, Table 1, Fig. 2(a). There is one exception in this series, namely the positions of $Eu_2MnGe_4O_{12}$ and $Gd_2MnGe_4O_{12}$ in the sequence which are inverted; the reason for it will be revealed below.

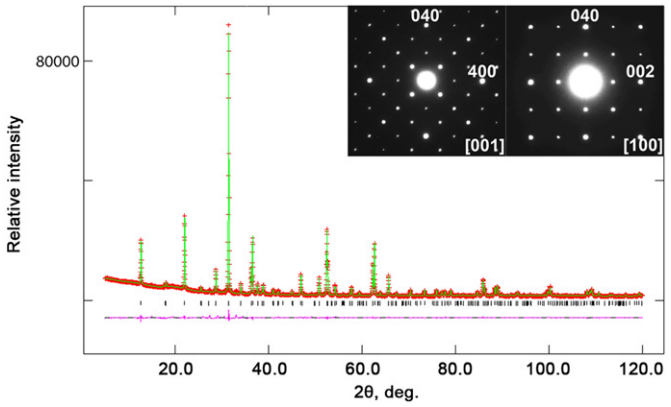

Fig. 1. Observed (crosses), calculated (solid line) and difference (bottom) powder diffraction pattern of $Ho_2CaGe_4O_{12}$ ($Ln_2MGe_4O_{12}$, where Ln=rare-earth element or Y; M=Ca, Mn, Zn). Inset: Selected area electron diffraction patterns of $Ho_2CaGe_4O_{12}$ recorded along [0 0 1]* and [1 0 0]*.

Attempts to obtain $Nd_2M^{2+}Ge_4O_{12}$ and $Pr_2M^{2+}Ge_4O_{12}$ were not successful, probably due to the relatively big size of Nd and Pr atoms ($r(Nd^{3+}(VI))$=1.123 Å, $r(Pr^{3+}(VI))$=1.13 Å) [13]. As an indirect evidence to corroborate this, the existence of the $CeMn_2Ge_4O_{12}$ compound, in which Mn atoms occupy only the octahedral 4f site while Ce^{4+} atoms ($r(Ce^{4+}(VI))$=1.11 Å) occupy only the 2b site, can be considered [12].

The EDX analyses of the samples showed that the obtained metal ratios were in good agreement with the nominal compositions. The structure of $Y_2CaGe_4O_{12}$ [8] was used as a starting model for the crystal structure refinement. For several samples $Ln_2Ge_2O_7$ has been included into the refinement as a second phase (Supporting Materials 1, CIF files and Figures). The peak profiles were fitted with a pseudo-Voigt function, $I(2\theta)=x\times L(2\theta)+(1-x)\times G(2\theta)$ (where L and G are the Lorentzian and Gaussian parts, respectively). The angular dependence of the peak width was described by the relation $(FWHM)^2=Utg^2\theta+Vtg\theta+W$, where $FWHM$ is the full line width at half maximum. The background level was described by a combination of thirty-six-order Chebyshev polynomials. The absorption correction function for a flat plate sample in transmission geometry has been applied [13]. At first the occupancies of the Ln(1) and Ln(2) positions have been varied with constrains keeping the chemical composition of the compound unchanged. During the refinement values of occupancies within the error margins converged to Ln:M^{2+}=0.5/0.5 and Ln:M^{2+}=1.0/0.0 for the Ln(1) and Ln(2) positions, respectively. At this point values of occupancies were fixed and not refined further. The crystallographic data, experimental details, R-values, atomic coordinates and displacement parameters are given in Tables 1–3. Analysis of Tables 2 and 3 shows that all compounds consist of two types of layers: layers of germanium tetracycles which alternate with calcium (manganese) – lanthanide layers (Fig. 3). The displacement parameters for heavy elements are larger than for oxygen (Tables 2 and 3). However, since X-ray powder diffraction is not an ideal method for precise determination of displacement parameters compared to, e.g. X-ray single crystal diffraction, we considered displacement factors more as a trimming parameter. Therefore, from their values we can evaluate the correctness of our model, but not real temperature factors (displacement factors).

The octahedra occupied by Ln and Ca(Mn) atoms are elongated along the directions to the O(1) atoms and shortened along the directions to the O(2) atoms. The average Ln(1)/Ca(Mn)–O distances in the octahedra are shortened with decreasing crystal radius of the rare-earth element, Fig. 2(b). In order to compare the degree of distortion of octahedra we considered the

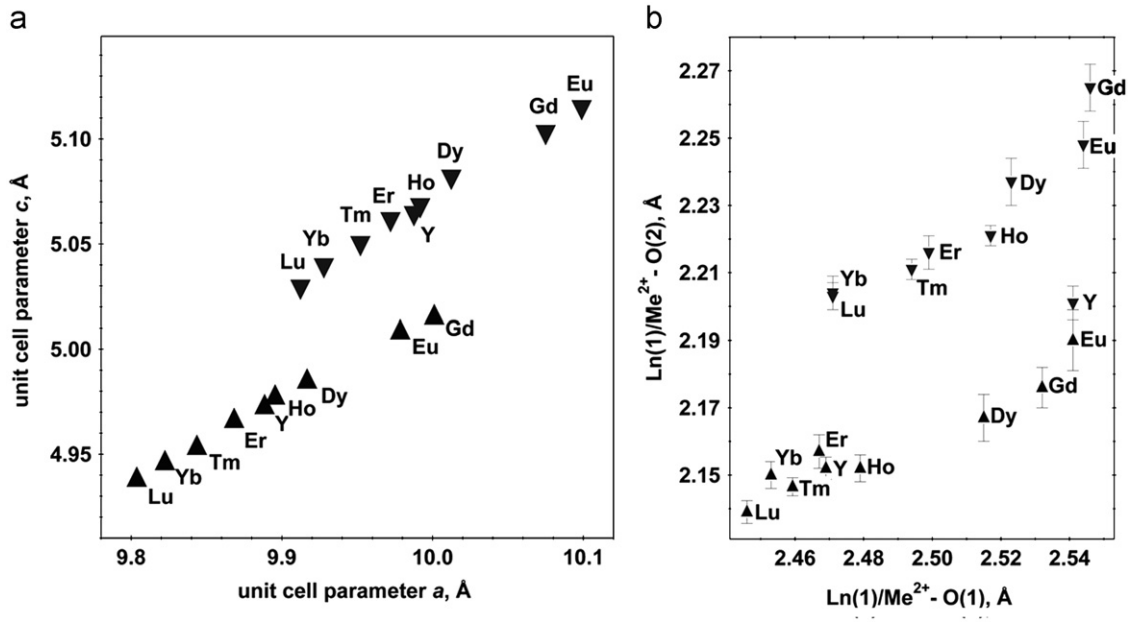

Fig. 2. (a) The variation of unit cell parameters and (b) the variation of ($Ln(1)/M^{2+}-O(1)$) and ($Ln(1)/M^{2+}-O(2)$) bond lengths in the $Ln_2MGe_4O_{12}$ compounds, where Ln=rare-earth element or Y; M=Ca, Mn (upturned triangles — for calcium compounds; triangles — for manganese compounds).

Table 1
Crystal data for $Ln_2M^{2+}Ge_4O_{12}$, M=Ca, Mn, Ln=Eu–Lu, Y.

	Eu	Gd	Dy	Ho	Er	Tm	Yb	Lu	Y
$Ln_2CaGe_4O_{12}$									
$a=b$, Å	10.09892(8)	10.07495(9)	10.0124(2)	9.99176(4)	9.97205(7)	9.9521(5)	9.92787(7)	9.9123(5)	9.98757(9)
c, Å	5.11491(5)	5.10301(6)	5.0817(1)	5.06810(2)	5.06150(4)	5.0501(3)	5.03951(4)	5.0293(3)	5.06434(6)
V, Å^3	521.660	517.979	509.431	505.975	503.325	500.184	496.707	494.147	505.175
Space group	*P4/nbm*	*P4/nbm*	*P4/nbm*	*P4/nbm*	*P4/nbm*	*P4/nbm*	*P4/nbm*	*P4/nbm*	*P4/nbm*
Formula units, Z	2	2	2	2	2	2	2	2	2
R_{wp}, R_p, %	2.34, 1.80	1.90, 1.48	2.19, 1.48	3.33, 2.25	5.07, 3.68	5.42, 3.93	6.43, 4.36	5.66, 3.85	5.79, 4.23
$R(F^2)$, %	5.29	3.26	4.14	2.34	2.42	2.00	2.67	2.41	3.51
$Ln_2MnGe_4O_{12}$									
$a=b$, Å	9.9785(5)	10.0011(5)	9.9167(5)	9.8955(5)	9.8683(5)	9.8436(2)	9.8224(5)	9.8037(2)	9.8885(5)
c, Å	5.0083(3)	5.0154(3)	4.9849(3)	4.9773(3)	4.9661(3)	4.9533(1)	4.9460(3)	4.9381(1)	4.9727(3)
V, Å^3	498.679	501.650	490.220	487.382	483.615	479.957	477.188	474.613	486.243
Space group	*P4/nbm*	*P4/nbm*	*P4/nbm*	*P4/nbm*	*P4/nbm*	*P4/nbm*	*P4/nbm*	*P4/nbm*	*P4/nbm*
Formula units, Z	2	2	2	2	2	2	2	2	2
R_{wp}, R_p, %	1.85, 1.46	1.49, 1.16	2.28, 1.54	3.25, 2.26	4.36, 3.24	2.58, 1.95	3.31, 2.25	3.01, 2.29	2.65, 1.90
$R(F^2)$, %	1.13	1.16	3.13	2.45	1.68	1.94	3.91	2.41	2.36

($Ln(1)/M^{2+}-O(1)$)/($Ln(1)/M^{2+}-O(2)$) ratio, Fig 2(b). For calcium germanates this parameter varies from 1.131(Eu) to 1.121 (Yb, Lu), and for manganese germanates from 1.161 (Eu) to 1.141 (Yb).

The $Ln(2)$–O(2) distances in square antiprisms also shorten with decreasing crystal radius of the rare-earth element. In the case of calcium germanates it changes from 2.419 Å (Eu) to 2.332 Å (Lu); these distances agree well with the theoretical values [14]. For manganese germanates the obtained values vary from 2.418 Å (Gd) to 2.308 Å (Lu) and are slightly smaller than the theoretical ones. The reduction of the Ln–O(2) bond lengths leads to a shortening of the O(2)–O(2) edge in the square antiprisms. In the ion bond approximation the theoretical values of the O(2)–O(2) distance cannot be less than 2.70 Å–2.84 Å [14]. Therefore, the four oxygen atoms O(2), which form the face of a square antiprism with edge O(2)–O(2) $\geq$ 2.84 Å in the *ab* plane, will not touch each other and the $[Ge_4O_{12}]^{8-}$ groups can be considered as discrete (isolated); if the length of the edge is shorter than 2.84 Å however, oxygen atoms will partly or fully touch each other, which would lead to the formation of two-dimensional networks of $[Ge_4O_{12}]^{8-}$. The described change can be considered as a transition of the structural motif from islands to two-dimensional networks. All obtained germanates have an island motif in the structure except $Lu_2CaGe_4O_{12}$, $Yb_2CaGe_4O_{12}$ and $Yb_2MnGe_4O_{12}$ in which $[Ge_4O_{12}]^{8-}$ groups form a two-dimensional network.

In the considered germanates the Ge–O(2) and Ge–O(1) bond lengths are close but the Ge–O(2) bond is always smaller, because bridge atom O(1) is connected with two neighboring germanium and one calcium (manganese) atom, whereas terminal O(2) is connected with one neighboring germanium atom and other distant cations (one Ln and one Mn). The ionic radius of the Ln^{3+} ion does not affect the lengths of these bonds, but it does affect the angles Ge–O(1) –Ge, changing the degree of distortion of the $[Ge_4O_{12}]$ cycle. It is interesting to compare this angle in germanates and isostructural vanadates $A_2SrV_4O_{12}$, where A=alkaline metal. In the case of vanadates the values of the V–O(1)–V angles vary from 127.8° (Na) to 157° (Cs) [15].

Table 2
Atomic coordinates and isotropic displacement parameters ($U_{iso} \times 100$, Å^2) for $Ln_2CaGe_4O_{12}$, Ln=Eu–Lu, Y.

		Eu	Gd	Dy	Ho	Er	Tm	Yb	Lu	Y
Ln(1)	*x/a, y/b, z/c*	0, 0, 1/2								
	$U_{iso} \times 100$	2.28(9)	4.32(4)	3.17(4)	2.68(2)	3.70(1)	3.30(7)	3.02(2)	2.85(6)	2.7(1)
Ln(2)	*x/a, y/b, z/c*	1/4, 1/4, 1/2								
	$U_{iso} \times 100$	1.72(9)	4.32(3)	2.90(8)	2.68(8)	3.70(1)	3.29(7)	3.02(1)	2.86(4)	2.7(1)
Ge	*x/a*	0.5238(2)	0.5233(2)	0.5221(1)	0.5213(1)	0.5208(1)	0.5202(1)	0.5201(1)	0.5194(1)	0.5207(2)
	y/b, z/c	1/4, 0								
	$U_{iso} \times 100$	2.15(8)	3.52(3)	2.82(9)	1.93(2)	2.93(1)	2.98(6)	2.49(2)	2.47(6)	2.45(9)
O(1)	*x/a*	−0.3727(6)	−0.3710(8)	−0.3720(6)	−0.3728(5)	−0.3712(3)	−0.3726(3)	−0.3742(5)	−0.3736(4)	−0.3714(6)
	y/b	0.3727(6)	0.3710(8)	0.3720(6)	0.3728(5)	0.3712(3)	0.3726(3	0.3742(5)	0.3736(4)	0.3714(6)
	z/c	0.152(1)	0.155(2)	0.155(1)	0.158(1)	0.1568(7)	0.156(1)	0.157(1)	0.1577(9)	0.149(1)
	$U_{iso} \times 100$	0.94(3)	2.60(8)	1.79(9)	1.65(5)	2.44(3)	2.40(8)	2.03(6)	2.24(9)	1.9(3)
O(2)	*x/a*	0.1753(6)	0.1762(6)	0.1742(6)	0.1739(5)	0.1736(3)	0.1732(3)	0.1733(5)	0.1734(4)	0.1740(5)
	y/b	0.0590(6)	0.0613(6)	0.0619(5)	0.0630(4)	0.0618(3)	0.0633(3)	0.0642(5)	0.0647(3)	0.0612(5)
	z/c	0.255(1)	0.252(1)	0.2531(9)	0.2559(8)	0.2566(5)	0.2567(7)	0.258(1)	0.2576(9)	0.2619(9)
	$U_{iso} \times 100$	1.32(2)	2.67(7)	2.06(7)	1.71(4)	2.44(2)	2.44(9)	1.92(4)	2.11(8)	1.9(3)

Ln(1)=0.5 × *Ln*(1)+0.5 × Ca.

Table 3
Atomic coordinates and isotropic displacement parameters ($U_{iso} \times 100$, Å^2) for $Ln_2MnGe_4O_{12}$, Ln=Eu–Lu, Y.

		Eu	Gd	Dy	Ho	Er	Tm	Yb	Lu	Y
Ln(1)	*x/a, y/b, z/c*	0, 0, 1/2								
	$U_{iso} \times 100$	2.4(1)	3.2(1)	4.5(1)	3.33(8)	2.15(5)	3.23(5)	3.04(7)	2.10(5)	1.90(7)
Ln(2)	*x/a, y/b, z/c*	1/4, 1/4, 1/2								
	$U_{iso} \times 100$	1.5(1)	2.7(1)	4.2(2)	3.08(9)	1.72(6)	2.67(5)	2.56(8)	1.44(6)	1.50(7)
Ge	*x/a*	0.9765(2)	0.9758(1)	0.9780(2)	0.9780(1)	0.9785(1)	0.9792(1)	0.9793(1)	0.9800(1)	0.9782(1)
	y/b, z/c	1/4, 0								
	$U_{iso} \times 100$	2.1(1)	2.6(1)	3.8(1)	2.75(8)	1.74(5)	2.70(5)	2.53(7)	1.63(5)	1.70(6)
O(1)	*x/a*	0.1324(8)	0.1328(5)	0.1317(7)	0.1312(4)	0.1307(5)	0.1305(3)	0.1304(4)	0.1309(4)	0.1308(3)
	y/b	0.8676(8)	0.8672(5)	0.8683(7)	0.8688(4)	0.8693(5)	0.8695(3)	0.8696(4)	0.8691(4)	0.8692(3)
	z/c	0.844(2)	0.838(2)	0.842(2)	0.835(1)	0.834(1)	0.8345(7)	0.834(1)	0.8318(8)	0.8333(8)
	$U_{iso} \times 100$	2.1(4)	2.0(3)	1.6(3)	1.8(2)	1.2(2)	2.0(1)	1.8(2)	1.2(1)	1.0(1)
O(2)	*x/a*	0.1694(8)	0.1685(5)	0.1688(7)	0.1687(4)	0.1695(5)	0.1685(2)	0.1694(4)	0.1689(3)	0.1689(3)
	y/b	0.0625(7)	0.0593(5)	0.0629(6)	0.0623(3)	0.0638(5)	0.0647(2)	0.0657(4)	0.0655(3)	0.0626(3)
	z/c	0.252(2)	0.252(1)	0.254(1)	0.2569(8)	0.257(1)	0.2571(5)	0.2577(8)	0.2586(6)	0.2571(6)
	$U_{iso} \times 100$	1.5(3)	1.5(2)	3.0(2)	2.1(1)	1.2(2)	2.0(1)	1.9(1)	1.2(1)	1.0(1)

Ln(1)=0.5 × *Ln*(1)+0.5 × Mn.

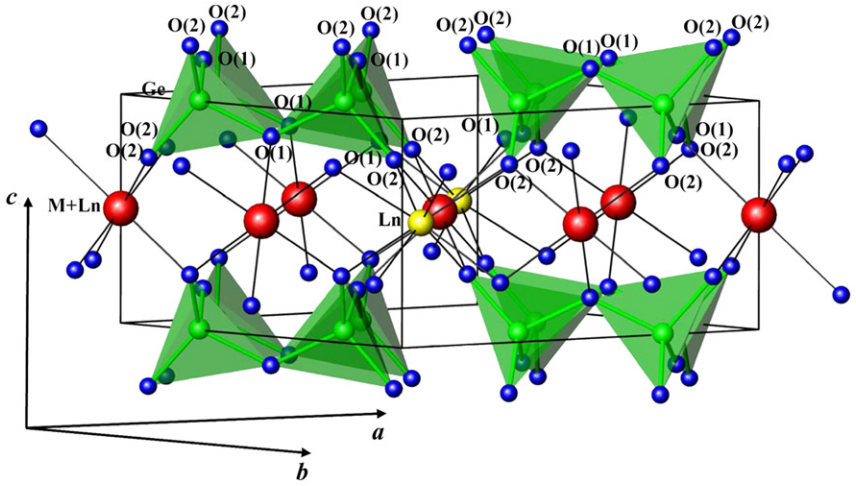

Fig. 3. Crystal structure of $Ln_2M^{2+}Ge_4O_{12}$, where Ln=rare-earth element or Y; M=Ca, Mn, Zn.

Table 4
Selected interatomic distances (Å) and bond angels (°) for $Ln_2CaGe_4O_{12}$, *Ln*=Eu–Lu, Y.

	Eu	Gd	Dy	Ho	Er	Tm	Yb	Lu	Y
Interatomic distances									
Ln(1)/Ca–O(1)	2 × 2.544(8)	2 × 2.546(8)	2 × 2.523(7)	2 × 2.517(4)	2 × 2.499(7)	2 × 2.494(4)	2 × 2.471(8)	2 × 2.471(5)	2 × 2.541(8)
Ln(1)/Ca–O(2)	4 × 2.248(7)	4 × 2.265(7)	4 × 2.237(7)	4 × 2.221(3)	4 × 2.216(5)	4 × 2.211(3)	4 × 2.204(5)	4 × 2.203(4)	4 × 2.201(5)
⟨***Ln*(1)/Ca–O**⟩	***2.347***	***2.359***	***2.332***	***2.319***	***2.308***	***2.307***	***2.293***	***2.292***	***2.314***
	2.334	*2.329*	*2.306*	*2.310*	*2.305*	*2.300*	*2.294*	*2.291*	*2.310*
Ln(2)–O(2)	*8 × 2.419(6)*	8 × 2.402(6)	8 × 2.388(5)	8 × 2.376(3)	8 × 2.361(5)	8 × 2.356(3)	8 × 2.340(5)	8 × 2.332(4)	*8 × 2.364(6)*
	2.426	*2.413*	*2.387*	*2.375*	*2.364*	*2.354*	*2.345*	*2.337*	*2.369*
Ge–O(1)	2 × 1.799(3)	2 × 1.802(4)	2 × 1.798(3)	2 × 1.803(2)	2 × 1.806(2)	2 × 1.801(2)	2 × 1.802(3)	2 × 1.804(2)	2 × 1.789(4)
Ge–O(2)	2 × 1.725(5)	2 × 1.713(6)	2 × 1.714(5)	2 × 1.717(2)	2 × 1.722(4)	2 × 1.718(3)	2 × 1.722(5)	2 × 1.718(3)	2 × 1.733(5)
⟨**Ge–O**⟩	***1.762***	**1.757**	***1.756***	**1.760**	**1.764**	**1.760**	**1.762**	**1.761**	***1.761***
	1.74	*1.74*	*1.74*	*1.74*	*1.74*	*1.74*	*1.74*	*1.74*	*1.74*
Bond angles									
O(1)GeO(1)	108.9(6)	107.5(7)	107.8(5)	107.6(3)	108.1(5)	107.3(3)	108.8(5)	108.0(3)	105.9(5)
O(1)GeO(2)	2 × 107.9(4)	2 × 109.3(5)	2 × 108.4(5)	2 × 108.9(3)	2 × 108.5(3)	2 × 108.3(2)	2 × 108.2(3)	2 × 108.5(2)	2 × 108.1(3)
O(1)GeO(2)	2 × 104.8(3)	2 × 104.9(4)	2 × 105.0(3)	2 × 104.6(2)	2 × 104.6(2)	2 × 105.1(2)	2 × 104.7(3)	2 × 104.7(2)	2 × 105.0(3)
O(2)GeO(2)	122.0(5)	120.7(5)	121.2(4)	122.1(2)	121.9(3)	122.1(2)	122.2(3)	121.9(3)	121.9(5)
⟨**OGeO**⟩	**109.4**	**109.4**	**109.4**	**109.4**	**109.4**	**109.4**	**109.4**	**109.4**	**109.4**
GeO(1)Ge	127.9(4)	127.4(5)	127.6(4)	127.3(2)	127.0(3)	127.8(3)	127.1(4)	127.2(3)	126.3(5)

Average values are given in boldface, theoretical values in Italic.

Table 5
Selected interatomic distances (Å) and bond angels (°) for $Ln_2MnGe_4O_{12}$, *Ln*=Eu–Lu, Y.

	Eu	Gd	Dy	Ho	Er	Tm	Yb	Lu	Y
Interatomic distances									
Ln(1)/Mn–O(1)	2 × 2.541(10)	2 × 2.532(7)	2 × 2.515(8)	2 × 2.479(5)	2 × 2.467(7)	2 × 2.459(3)	2 × 2.453(5)	2 × 2.446(4)	2 × 2.469(4)
Ln(1)/Mn–O(2)	4 × 2.190(9)	4 × 2.176(6)	4 × 2.167(7)	4 × 2.152(4)	4 × 2.157(5)	4 × 2.146(3)	4 × 2.150(4)	4 × 2.139(3)	4 × 2.152(3)
⟨***Ln*(1)/Mn–O**⟩	***2.307***	***2.295***	***2.283***	***2.261***	***2.260***	***2.281***	***2.251***	***2.241***	***2.258***
	2.249	***2.244***	***2.231***	***2.226***	***2.220***	*2.215*	***2.209***	***2.206***	***2.225***
Ln(2)–O(2)	*8 × 2.386(7)*	8 × 2.418(5)	8 × 2.366(6)	8 × 2.359(4)	8 × 2.338(5)	8 × 2.328(3)	8 × 2.312(4)	8 × 2.308(3)	8 × 2.353(3)
	2.426	*2.413*	*2.387*	*2.375*	*2.364*	*2.354*	*2.345*	*2.337*	*2.369*
Ge–O(1)	2 × 1.780(4)	2 × 1.792(3)	2 × 1.783(4)	2 × 1.797(2)	2 × 1.795(3)	2 × 1.795(2)	2 × 1.793(2)	2 × 1.799(2)	2 × 1.799(2)
Ge–O(2)	2 × 1.724(6)	2 × 1.722(5)	2 × 1.721(6)	2 × 1.725(4)	2 × 1.723(5)	2 × 1.725(2)	2 × 1.724(4)	2 × 1.722(3)	2 × 1.724(3)
⟨**Ge–O**⟩	***1.752***	**1.757**	***1.752***	**1.761**	**1.759**	**1.760**	**1.758**	**1.761**	***1.762***
	1.740	*1.74*	***1.74***	***1.74***	***1.74***	*1.74*	***1.74***	*1.74*	***1.74***
Bond angles									
O(1)GeO(1)	104.8(7)	105.4(5)	104.8(6)	106.0(3)	106.2(5)	106.0(2)	106.1(4)	105.6(3)	106.4(3)
O(1)GeO(2)	2 × 108.5(5)	2 × 108.5(3)	2 × 108.4(4)	2 × 109.0(2)	2 × 109.3(3)	2 × 109.0(2)	2 × 109.5(3)	2 × 109.7(2)	2 × 109.1(2)
O(1)GeO(2)	2 × 106.9(4)	2 × 105.7(3)	2 × 106.3(3)	2 × 104.8(2)	2 × 104.8(3)	2 × 105.1(2)	2 × 104.9(2)	2 × 104.5(2)	2 × 104.7(2)
O(2)GeO(2)	120.2(6)	122.0(4)	121.4(5)	122.2(3)	121.5(4)	121.6(2)	121.1(3)	121.8(2)	122.1(2)
⟨**OGeO**⟩	**109.3**	**109.3**	**109.3**	**109.3**	**109.3**	**109.3**	**109.3**	**109.3**	**109.4**
GeO(1)Ge	127.7(6)	126.1(4)	127.4(5)	125.22(28)	125.2(4)	125.4(2)	125.4(3)	124.9(2)	124.93(22)

Average values are given in boldface, theoretical values in Italic.

Comparison of these values with the data of Tables 4 and 5 allows to conclude that:

(a) the geometrical shape of cycles in $Ln_2CaGe_4O_{12}$ and $Na_2SrV_4O_{12}$ is similar and differs from $A_2SrV_4O_{12}$, A=K, Rb, Cs;
(b) the shape of the cycles mostly depends on the radius of the cation in the octahedral site.

The above-described structure of cycles, which consists of four GeO_2 groups (oxygen atoms are placed above and under the plane of the cycle) connected by means of Ge–O–Ge bridge bonds, can be regarded as a harmonic oscillator upon inelastic scattering of exciting radiation. This feature is most interesting in the case of $Y_2CaGe_4O_{12}$ and $Y_2MnGe_4O_{12}$ due to their promising use as an optical host for creating new phosphors. A rare-earth cation, substituted in these hosts, can act as an activator and as a sensitizer. In order to determine the optimal concentration of rare-earth ions at which maximal luminescence can be achieved and also to study the tendency of rare-earth elements to occupy six- or eight-coordinated sites in the structure, different solid solutions were synthesized for the first time.

3.2. Crystal structure of solid solutions based on $Y_2CaGe_4O_{12}$, $Y_2MnGe_4O_{12}$ and $Y_2ZnGe_4O_{12}$ matrices

Iso- and heterovalent substitution has been studied on samples of the $Y_{2-x}Er_xCaGe_4O_{12}$ (x=0–2), $Y_{2-2x}Ce_xCa_{1+x}Ge_4O_{12}$ (x=0–1) and $Y_{2-x}Pr_xMnGe_4O_{12}$ (x=0–0.5) solid solutions. For all solid solutions a smooth change of the unit cell parameters and volume in the whole range of x has been observed (Fig. 4(a)). The full profile structure refinement procedure reveals that in $Y_{2-x}Er_xCaGe_4O_{12}$, Er^{3+} ions occupy both eight- and six-coordinated sites, but mainly the *2b* site with antiprismatic configuration and less the octahedral *4f* site, with an average ratio of 0.7/0.3 (Fig. 4(b)). In the $Y_{2-2x}Ce_xCa_{1+x}Ge_4O_{12}$ (x=0–1) solid solution Ce^{4+} ions occupy only *2b* sites with antiprismatic configuration (Fig. 4(c)).

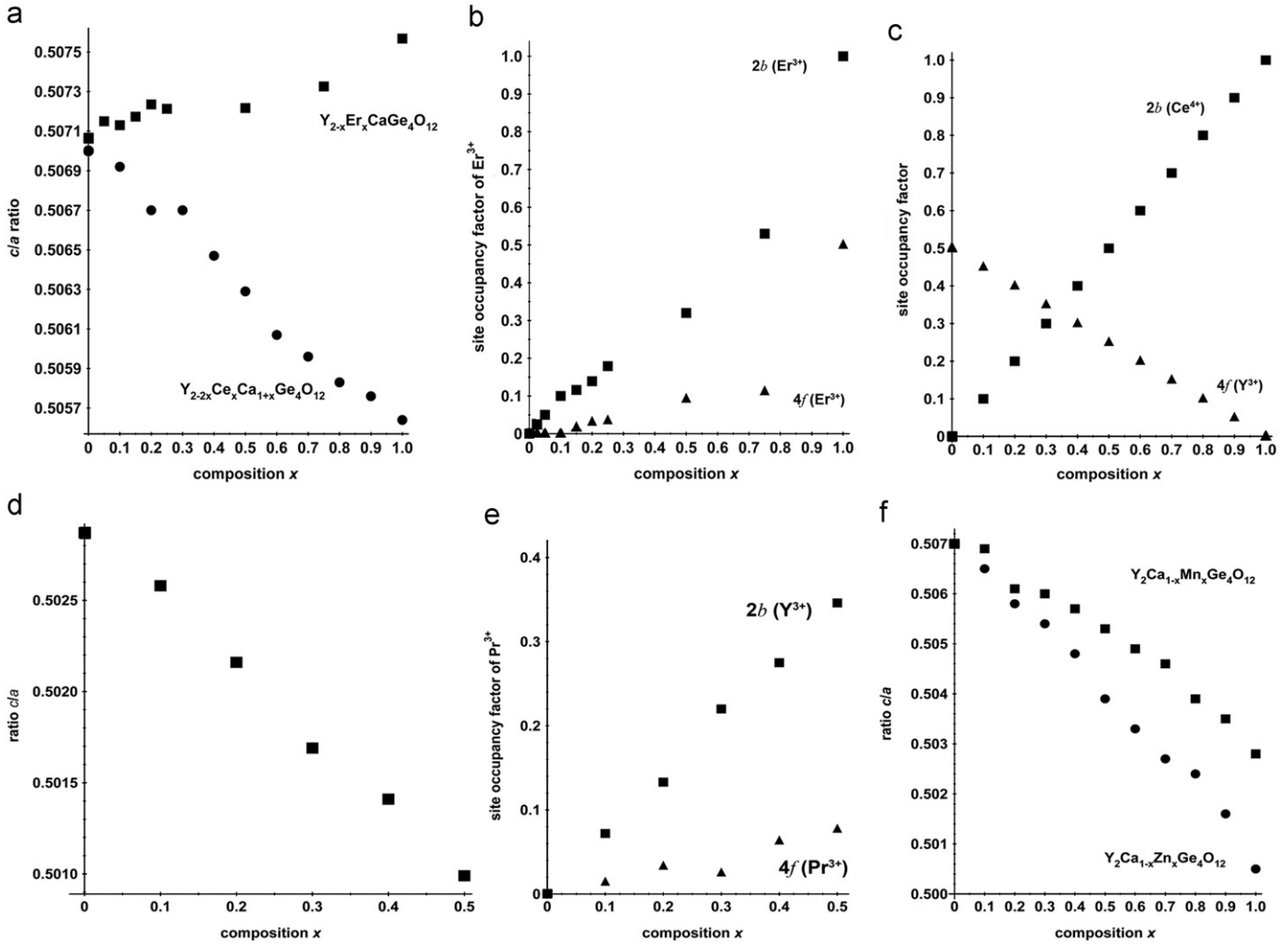

Fig. 4. (a) Dependence of the c/a ratio on x for $Y_{2-x}Er_xCaGe_4O_{12}$ and $Y_{2-2x}Ce_xCa_{1+x}Ge_4O_{12}$ solid solutions; (b) dependence of site occupancy factors of Er^{3+} on x (x=0–1) for the $Y_{2-x}Er_xCaGe_4O_{12}$ solid solution; (c) dependence of site occupancy factors of Ce^{4+} and Y^{3+} on x (x=0–1) for the $Y_{2-2x}Ce_xCa_{1+x}Ge_4O_{12}$ solid solution; (d) Change of unit cell parameters with x for the $Y_{2-x}Pr_xMnGe_4O_{12}$ solid solution; (e) dependence of site occupancy factors of Pr^{3+} on x (x=0–0.5) for the $Y_{2-x}Pr_xMnGe_4O_{12}$ solid solution; (f) change of unit cell parameters with x for the $Y_2Ca_{1-x}Mn_xGe_4O_{12}$ and $Y_2Ca_{1-x}Zn_xGe_4O_{12}$ solid solutions.

While $Nd_2M^{2+}Ge_4O_{12}$ and $Pr_2M^{2+}Ge_4O_{12}$ could not be obtained by means of the described synthesis procedure, Pr^{3+} ions can be substituted into the $Y_2MnGe_4O_{12}$ matrix. The $Y_{2-x}Pr_xMnGe_4O_{12}$ solid solution in the range $0 \le x \le 0.5$ has been studied (Fig. 4(d)). Pr^{3+} ions occupy both six- and eight-coordinated sites, but mainly the *2b* site with the same tendency as it was found for $Y_{2-x}Er_xCaGe_4O_{12}$ (Fig. 4(e)).

Since manganese can change its oxidation state, the $Y_2MnGe_4O_{12}$ matrix is more flexible for doping, allowing substitution with dopants which can not be introduced into the $Y_2CaGe_4O_{12}$ matrix directly. Therefore, it was important to check the possibility of obtaining a solid solution in between the two considered matrices $Y_2CaGe_4O_{12}$ and $Y_2MnGe_4O_{12}$. It has been shown that these matrices form the continuous solid solution $Y_2Ca_{1-x}Mn_xGe_4O_{12}$ (x=0–1), Fig. 4(f).

The possibility to substitute Ca by Zn has been checked. The continuous solid solution $Y_2Ca_{1-x}Zn_xGe_4O_{12}$ (x=0–1) has been found (Fig. 4(f)). $Y_2ZnGe_4O_{12}$ was synthesized for the first time.

It has been shown that the full substitution of Ca by Zn leads to a c/a ratio almost equal to 0.5, but the Ge_4O_{12} cycles do not change symmetry from a 2-fold to a 4-fold axis as it was found for cesium cyclovanadate [15]. In vanadates, Cs occupies the 4*f* position, the O(1) atoms lie in the same plane as the vanadium atoms, the O(2) atoms in each tetrahedra are lined up along the z axis which changes the crystal symmetry from *P*4/*nbm* to *P*4/*mmm*. However, in the case of germanates the octahedral symmetry around the 4*f* position is preserved and does not lead to a twist of the tetrahedra and to a transition to the *P*4/*mmm* space group (Fig. 5).

3.3. Electron spin resonance and magnetic property measurements

For the whole set of the $Ln_2MnGe_4O_{12}$, Ln=Eu–Lu, Y germanates electron spin resonance spectra have been registered at room temperature. Each sample, except $Lu_2MnGe_4O_{12}$, contains two different magnetic ions: a rare-earth ion and manganese. However, it is known [16] that ESR spectra of rare-earth ions with electron configuration $f^n \neq f^7$ can be detected only at temperatures near liquid helium due to very short relaxation time. Therefore, the spectra of the samples which contain such rare-earth elements exhibit only a single symmetrical line (line width ~2000–2300 G) with g=2, which is typical for Mn^{2+} ions. The $Gd_2MnGe_4O_{12}$ sample gives a noticeably higher intensity of the signal and less broadening of the line in the spectrum, since it is formed by the superposition of the signals from Mn^{2+} and Gd^{3+} (f^7-ion). It was expected that the $Eu_2MnGe_4O_{12}$ sample should have the same spectrum as all other samples containing rare-earth elements with electron configuration $f^n \neq f^7$. However, the

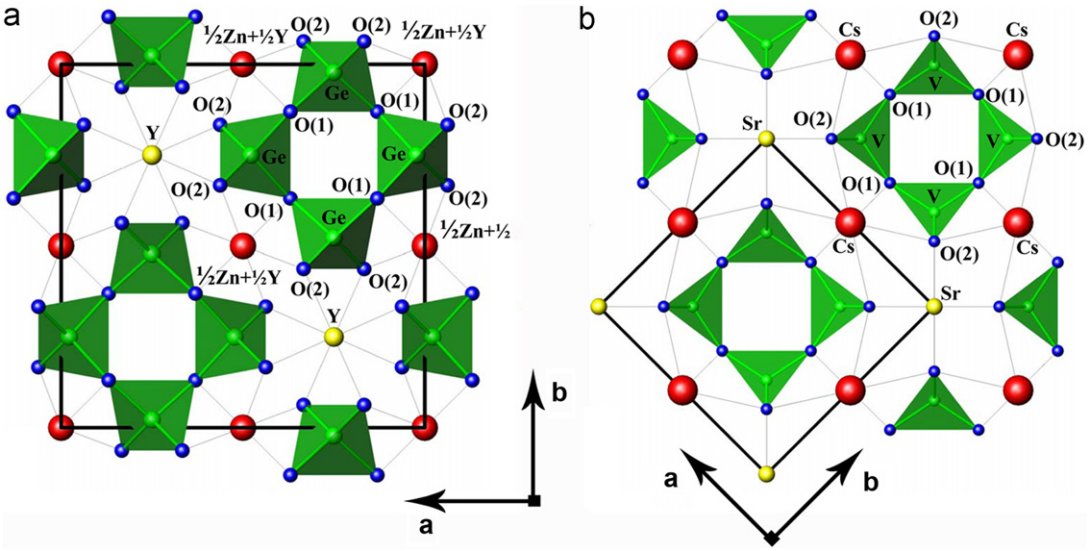

Fig. 5. View along the c direction of the crystal structure of (a) $Y_2ZnGe_4O_{12}$ and (b) $Cs_2SrV_4O_{12}$.

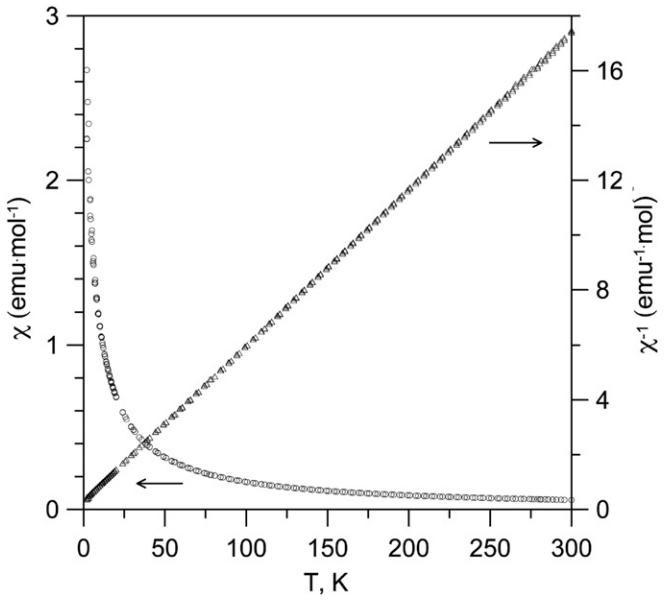

Fig. 6. Thermal evolution of the molar magnetic susceptibility (χ) and its reciprocal (χ^{-1}) for $Eu_2MnGe_4O_{12}$.

spectrum has a line with intensity comparable to $Gd_2MnGe_4O_{12}$ with $g=2.04$, which indicates the presence of Eu^{2+} ions in the structure.

In order to get additional information on magnetic properties and to reveal the oxidation state of europium and manganese in $Eu_2MnGe_4O_{12}$ the magnetic susceptibility curve was measured in the temperature range 1.5–300 K (Fig. 6). A linear temperature dependence of the reciprocal molar magnetic susceptibility was found. Hence, the magnetic behavior of this germanate follows a Curie–Weiss law: $\chi=A_0+C/(T-\Theta)$, where A_0 is a temperature independent part including both diamagnetic and Van Vleck paramagnetic components, C is the Curie constant, and Θ the Weiss temperature. Fitted parameters are: $A_0=0.014\,cm^3\,mol^{-1}$, $C=13.65\,cm^3\,K\,mol^{-1}$, $\Theta=-2.9\,K$. The effective magnetic moment of one mol of $Eu_2MnGe_4O_{12}$ is related to the Curie constant in the following way: $\mu^2_{eff}=8C$. On the other hand $\mu^2_{calc}=\sum\mu_i^2\mu_B$, where the index "$i$" numbers different paramagnetic centers which are contained in one mol of $Eu_2MnGe_4O_{12}$. To draw a conclusion about the valence state of Eu and Mn ions in $Eu_2MnGe_4O_{12}$ it is necessary to consider possible combinations of μ_i^2 and to compare them with the experimental value of $\mu^2_{eff}=109.2\ \mu^2_B$. For Mn^{2+} ($3d^5$) and Mn^{4+}($3d^3$) ions theoretical spin-only moments can be written as $\mu=2\sqrt{[S(S+1)]}$: $\sqrt{35}\ \mu_B$ and $\sqrt{15}\ \mu_B$, respectively. The case of Mn^{3+} ($3d^4$) in the applied synthesis conditions seems to be not realizable. Magnetic moments for rare-earth ions are calculated with the formula $\mu=g\sqrt{[J(J+1)]}$, and for Eu^{2+} ($4f^7$) and Eu^{3+} ($4f^6$) should be equal to 7.9 μ_B and 0, respectively. However, for Eu^{3+}, low-lying multiplets give rise to both a Van Vleck contribution and to a thermal occupation of the exited term. As a result Eu^{3+} has a nonzero magnetic moment. Usually μ^{3+}_{Eu} is about 3–3.5 μ_B (e.g. 3.14 μ_B in Ref. [17]). Taking these values into account one can determine $\sum\mu_i^2$ for two boundary cases: for $Eu_2^{3+}Mn^{2+}Ge_4O_{12}$, $\sum\mu_i^2=58.1\ \mu_B^2$ and for $Eu_2^{2+}Mn^{4+}Ge_4O_{12}$, $\sum\mu_i^2=139.8\ \mu_B^2$. The second case is more realistic, nevertheless the calculated value $\sum\mu_i^2$ differs noticeably from the experimental value μ^2_{eff}. We suppose that the europium in $Eu_2MnGe_4O_{12}$ is mainly divalent but that there is some fraction of Eu^{3+} ions. For the charge compensation a part of manganese has to be in the Mn^{2+} state with the Mn^{2+}/Eu^{3+} ratio equal to 1/2. So, the observed value of $\mu^2_{eff}=109.2\ \mu_B^2$ corresponds approximately to $Eu^{2+}_{1.3}Eu^{3+}_{0.7}Mn^{4+}_{0.65}Mn^{2+}_{0.35}Ge_4O_{12}$. This formula representation reflects both the magnetic moment and valence balances but does not allow to judge about the occupation of six- or eight-coordinated sites with Eu^{2+} and Eu^{3+}ions. The reduction of Eu^{3+} to Eu^{2+} in air has been observed in other systems as well [18,19], but the possible explanation of this process proposed in Ref. [19] can hardly be applied for the $Eu^{2+}_{1.3}Eu^{3+}_{0.7}Mn^{4+}_{0.65}Mn^{2+}_{0.35}Ge_4O_{12}$ compound, and is a topic for a following study. Since the ion pair Eu^{2+} and Mn^{2+} is known as a promising activator for optical devices which convert ultraviolet to visible light (UV LEDs (light-emitting diodes)) [20,21], we propose $Eu_2MnGe_4O_{12}$ as a dopant for the optical host based on the cyclic germanates described above.

4. Conclusions

The crystal structure of the promising optical materials $Ln_2M^{2+}Ge_4O_{12}$, where Ln=rare-earth element or Y; M=Ca, Mn, Zn and their solid solutions has been studied in detail. It has been shown that choosing the doping element one can control

iso- and heterovalent substitution in $Y_2CaGe_4O_{12}$, $Y_2MnGe_4O_{12}$, $Y_2ZnGe_4O_{12}$ and $CeCa_2Ge_4O_{12}$ hosts and optimize the composition of the considered optical materials. The capability of cyclic germanates to form solid solutions with both iso- and heterovalent substitution is similar to those for compounds crystallized in perovskite, spinel and garnet structure types.

Acknowledgments

This work was supported by the Russian Foundation for Basic Research under Grant no. 07-03-00143a, 10-03-96028 r_ural_a, and Grant no. 09-P-3-1009, sponsored by UB RAS.

Appendix A. Supplementary material

Supplementary data associated with this article can be found in the online version at doi:10.1016/j.jssc.2010.03.027.

References

[1] C. Ronda, Luminescence: From Theory to Applications, WILEY-VCH, Weinheim, 2008.
[2] A.J. Kenyon, Prog. Quant. Electron. 26 (2002) 225–284.
[3] J.A. Campa, C. Cascales, E. Gutierrez-Puebla, M.A. Monge, I. Rasines, C. Ruiz-Valero, J. Solid State Chem. 124 (1996) 17–23.
[4] C. Cascales, M.T. Fernandez Diaz, M.A. Monge, Chem. Mater. 12 (2000) 3369–3375.
[5] C. Cascales, M.A. Monge, J. Alloys Compd. 344 (2002) 379–384.
[6] E.J. Baran, C.C. Wagner, A.E. Lavat, C. Cascales, J. Raman Spectrosc. 28 (1997) 927–931.
[7] U. Lambert, W. Eysel, Powder Diffr. 1 (1986) 256–260.
[8] H. Yamane, R. Tanimura, T. Yamada, J. Takahashi, T. Kajiwara, M. Shimada, J. Solid State Chem. 179 (2006) 289–295.
[9] N.V. Tarakina, V.G. Zubkov, I.I. Leonidov, A.P. Tyutyunnik, L.L. Surat, J. Hadermann, G. Van Tendeloo, Z. Kristallogr. (Supplement) 30 (2009) 401–406.
[10] V.G. Zubkov, I.I. Leonidov, A.P. Tyutyunnik, N.V. Tarakina, L.A. Perelyaeva, I.V. Baklanova, L.L. Surat, Phys. Solid State 50 (2008) 1699–1706.
[11] V.G. Zubkov, I.I. Leonidov, A.P. Tyutyunnik, N.V. Tarakina, L.L. Surat, L.A. Perelyaeva, I.V. Baklanova, O.V. Koryakova, J. Lumin. 129 (2009) 1625–1628.
[12] C. Taviot-Gueho, P. Leone, P. Palvadeau, J. Rouxel., J. Solid State Chem. 143 (1999) 145–150.
[13] Larson, A.C. & Von Dreele, R.B., 2004, General Structure Analysis System (GSAS), Los Alamos: National Laboratory.
[14] R.D. Shannon, Acta Crystallogr. A 32 (1976) 751–767.
[15] B.V. Slobodin, L.L. Surat, V.G. Zubkov, A.P. Tyutyunnik, I.F. Berger, L.A. Perelyaeva, I.R. Shein, A.L. Ivanovskii, M.V. Kuznetsov, B.V. Shulgin, V.I. Solomonov, G. Svensson, B. Forslund, M.J. Sayagués, Phys. Rev. B Condens. Matter 72 (2005) 155205, 1–12.
[16] A. Abragam, B. Bleaney, Electron Paramagnetic Resonance of Transition Ions, Clarendon Press, Oxford, 1970.
[17] A. Butera, A. Fainstein, E. Winkler, J. Tallon, Phys. Rev. B Condens. Matter. 63 (2001) 054442, 1–5.
[18] M. Peng, G. Hong, J. Lumin. 127 (2007) 735–740.
[19] Z. Lian, J. Wang, Y. Lv, Sh. Wang, Q. Su, J. Alloys Compd. 430 (2007) 257–261.
[20] J. Garcia, W.A. Sibley, J. Lumin. 42 (1988) 109–116.
[21] U. Happek, A.A. Setlur, J.J. Shiang, J. Lumin. 129 (2009) 1459–1463.